Sinter-Resistant Catalysts

DOI: 10.1002/anie.201201726

A "Smart" Catalyst: Sinter-Resistant Supported Iridium Clusters Visualized with Electron Microscopy**

*Ceren Aydin, Jing Lu, Nigel D. Browning, and Bruce C. Gates**

Supported metal nanostructures are among the most important technological catalysts, used in processes ranging from 1) petroleum refining to 2) Fischer–Tropsch synthesis of hydrocarbon fuels and to 3) vehicle exhaust clean-up. The respective metals include 1) rhenium–platinum, iridium–platinum, and tin–platinum combinations; 2) cobalt; and 3) rhodium–platinum. The most efficient of these catalysts consist of small clusters or particles of metal with high surface areas dispersed on porous metal oxide supports.

The catalytic activity and selectivity of supported metal nanoclusters depend on their size, shape, and interactions with the support. Such catalysts lose activity in operation, often by aggregation (sintering) of the nanoclusters, with the attendant loss of surface area and changes in the electronic structure of the metal.[1–3] Deactivated catalysts typically have to be taken out of operation for regeneration by treatments that cause metal redispersion, such as by formation of volatile metal halides[4,5] that, after redeposition on the support, are treated to reform metal clusters.

Some supports are known to provide resistance to sintering by interacting strongly with metal nanoclusters, with notable industrial examples being perovskites and ceria.[6,7] The strong metal–support interactions in these systems, however, affect the electronic structure of the metal and therefore its catalytic performance.[8] As an alternative, metal nanoclusters can also be stabilized by partial encapsulation within oxides,[9–11] but at the cost of coverage of catalytic sites and loss of catalytic activity.[12] Furthermore, although these approaches slow down the sintering process, they do not prevent it, and, as yet, there are no examples of intrinsically stable supported metal catalysts that are sinter-resistant.

Here we report atomic-scale observations of oxide-supported iridium nanocluster catalysts that resist sintering because the clusters of a critical size do not coalesce. These are "smart" catalysts, the first with intrinsic properties that hinder the process of sintering that generally causes deactivation of supported metal catalysts.[13] Iridium nanoclusters are important catalysts because they are active for numerous reactions of hydrocarbons, including hydrogenation,[14,15] dehydrogenation,[16,17] and hydrogenolysis, including ring-opening of naphthenes, for which they offer unique properties that are markedly superior to those of other metals when the iridium nanocluster diameters are in the range of 0.6–1.6 nm.[18–22] MgO is an ideal support to test the catalytic properties of iridium nanoclusters because it is highly stable and has a high surface area that is consistent with the needs of many industrial catalysts.

MgO-supported iridium catalysts were prepared by the reaction of $Ir(C_2H_4)_2(acac)$ (acac is acetylacetonate) with hydroxy groups of the support.[23] Infrared (IR) and extended X-ray absorption fine structure (EXAFS) spectra of the initially prepared catalyst show the presence of mononuclear iridium diethene complexes anchored to the MgO surface through $Ir{-}O_{support}$ bonds;[24] images of the catalyst obtained by aberration-corrected scanning transmission electron microscopy (STEM) confirm the atomic dispersion and site-isolation of the iridium species.[24] These supported species are readily reduced and aggregated to form iridium nanoclusters on the support—exposure of the sample to H_2 under mild conditions (353 K and 1 bar for 1 h) leads to the formation of Ir_4 clusters (Figure S1 in the Supporting Information).[25] Treatment in H_2 at higher temperatures leads to the formation of clusters larger than Ir_4, but, strikingly, treatment at 673 K for 8 h leads only to the formation of iridium nanoclusters no larger than a critical size (Figure 1). The sample consisted of almost uniform nanoclusters with an average diameter of (1.04 ± 0.16) nm (corresponding to an average of approximately 40 Ir atoms per cluster[26]). The distribution of measured cluster diameters is explained by standard blurring effects in STEM images (associated with electron beam probe size, vibrational instabilities, irradiation effects, off-focus, beam broadening, etc.). These effects are expected to cause a slight overestimation of the cluster diameters in addition to a broadening of the size distribution.[27]

To test the stability of the supported nanoclusters, the sample was treated again in H_2, this time at a higher temperature, 873 K, for 8 h. Analysis of the STEM images showed that the nanoclusters had an average diameter of (0.96 ± 0.17) nm, matching the value characterizing the

[*] C. Aydin,[+] J. Lu,[+] Prof. N. D. Browning,[$] Prof. B. C. Gates
Department of Chemical Engineering and Materials Science
University of California, Davis, CA 95616 (USA)
E-mail: bcgates@ucdavis.edu
Homepage: http://www.chms.ucdavis.edu/research/web/catalysis

[$] Current address:
Fundamental and Computational Sciences Division
Pacific Northwest National Laboratory
Richland, WA 99352 (USA)

[+] These authors contributed equally to this work.

[**] This work was supported by the Department of Energy (DOE) Basic Energy Sciences grant number DE-FG02-03ER46057 (C.A.) and grant number DE-SC0005822 (J.L.) and the University of California Lab Fee Program. We acknowledge beam time and the support of the DOE Division of Materials Sciences for its role in the operation and development of beam line 4–1 at the Stanford Synchrotron Radiation Lightsource. We thank the beamline staff for valuable support.

Supporting information for this article is available on the WWW under http://dx.doi.org/10.1002/anie.201201726.

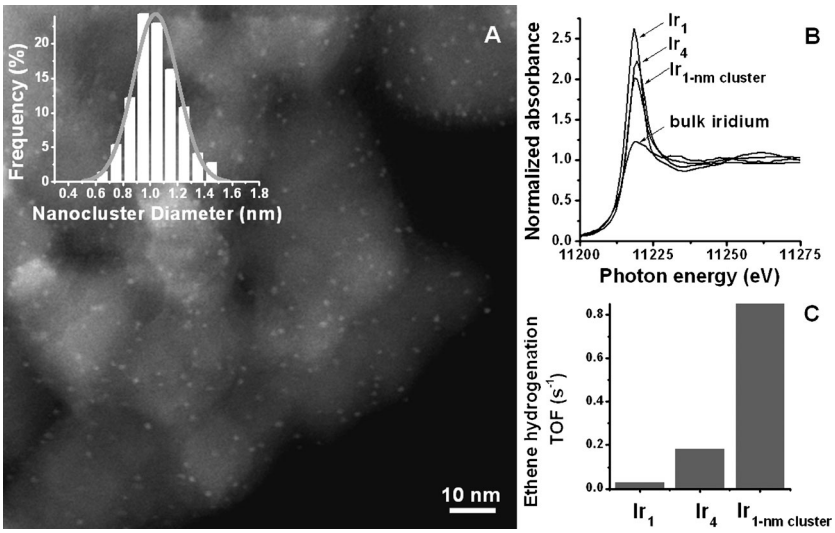

Figure 1. Characterization and catalytic activity of a sample containing supported iridium nanoclusters prepared by treating $Ir(C_2H_4)_2$ complexes on MgO in flowing H_2 at 673 K for 8 h. A) High-angle annular dark-field (HAADF) STEM image and histogram showing the distribution of nanocluster diameters (inset). B) Normalized XANES spectra at Ir L_{III} edge characterizing supported iridium complex, Ir_4 clusters, iridium clusters with an average diameter of approximately 1 nm, and iridium metal. C) Rate of ethene hydrogenation catalyzed by supported iridium complexes, Ir_4 clusters, and iridium nanoclusters with an average diameter of approximately 1 nm.

sample after the first (lower-temperature) H_2 treatment (Figure S2 in the Supporting Information). The results show that the iridium clusters are highly stable even under the more harsh reduction conditions.

The catalyst in all forms was active for ethene hydrogenation. The activity increased as the site-isolated mononuclear iridium complexes[25] were converted into Ir_4[25] and then into the nearly 1 nm nanoclusters formed in H_2 at 673 K (Figure 1 C). To explain this trend of increasing activity, we analyzed the X-ray absorption near-edge structure (XANES) spectra (Figure 1 B) characterizing the supported iridium complex, Ir_4 clusters, and iridium clusters of approximately 1 nm in diameter. The data show that the white line intensity characterizing the iridium clusters of approximately 1 nm in diameter is very similar to the white line intensities characterizing the iridium complex and Ir_4 clusters, which are significantly greater than that intensity characterizing the bulk iridium, indicating that the electronic properties of the iridium clusters of approximately 1 nm in diameter are closer to those of the molecular iridium complexes and clusters than to those of bulk iridium. The increase in hydrogenation activity with cluster nuclearity is expected in this case because of the ability of neighboring Ir atoms to activate multiple reactants.[25]

EXAFS data show clearly how the average Ir–Ir first-shell coordination number increased as aggregation progressed. The value increased from zero for the mononuclear iridium complex, to approximately 3 (2.9) for the Ir_4 clusters,[25] to 7.1 (with the appearance of a second-shell Ir–Ir contribution with a coordination number of 3.2) for the sample treated at 673 K (Table S1 in the Supporting Information). Consistent with the STEM images, the coordination number of 7.1 indicates approximately 40 Ir atoms per cluster, estimated on the basis of experimental correlations that presume a cubic structure.[28]

The aggregation of supported metal complexes and clusters starts with the migration of the metal species on the support surface, which must involve the breaking of metal–support bonds.[29] This process occurs not only in an H_2 atmosphere at elevated temperatures,[25,29] but also, as our images show, in the STEM under the influence of the electron beam.[30,31] The STEM images, showing that the iridium species are highly mobile on the surface of MgO, rule out the possibility that the stability of the iridium clusters of approximately 1 nm in diameter should be attributed to the limited mobility—and they provide a unique opportunity to track the aggregation process as it occurs and to investigate the origin of the stability of the clusters of approximately 1 nm in diameter. The images show that isolated Ir atoms and nanoclusters much smaller in diameter than 1 nm migrated and aggregated readily on the MgO surface—but, as was observed in the H_2 treatment, the aggregation stopped when the clusters reached this critical size. Critically sized clusters seemed to "bounce" off each other, as shown by sequential STEM images of the same areas

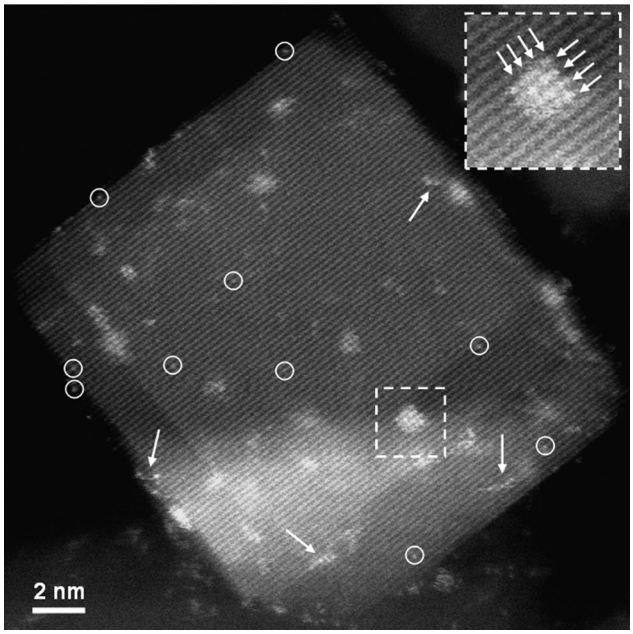

Figure 2. HAADF-STEM image of MgO-supported iridium species formed by the reaction of $Ir(C_2H_4)_2(acac)$ with the MgO surface followed by exposure to the electron beam (the imaging dose was approximately 10^5 e^- $Å^{-2}$) for 30 s. Examples of isolated Ir atoms are encircled; the arrow indicates aligned Ir atoms en route to cluster formation. A magnified view of the cluster in the square frame is shown in the inset.

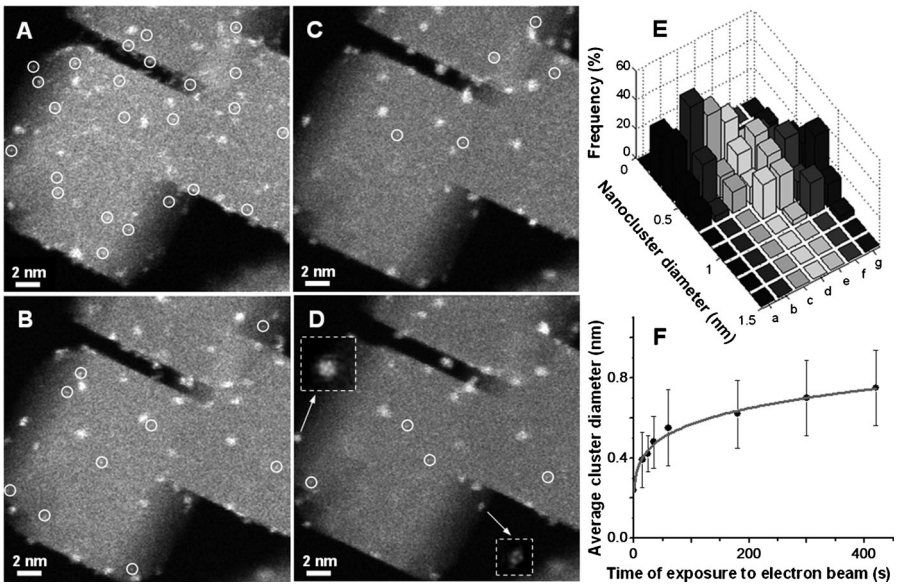

Figure 3. Evolution of iridium cluster size distribution during electron beam exposure. A–D) HAADF-STEM images of MgO-supported iridium sample after the following beam exposures (in min): A) 1, B) 3, C) 5, and D) 7. Examples of isolated Ir atoms are encircled, and magnified views of two individual clusters are shown in the inset of (D). E) Cluster size distribution following the exposure to the electron beam for the following times (in s): a) 15, b) 25, c) 35, d) 60, e) 180, f) 300, and g) 420. F) Evolution of the average cluster diameter during exposure to the beam (the error bars correspond to the standard deviations of the measurements). The electron dose received in the imaged area through the course of the captured movie was approximately (10^5–10^7) e^- Å^{-2} (see the Supporting Information for details of the dose calculations).

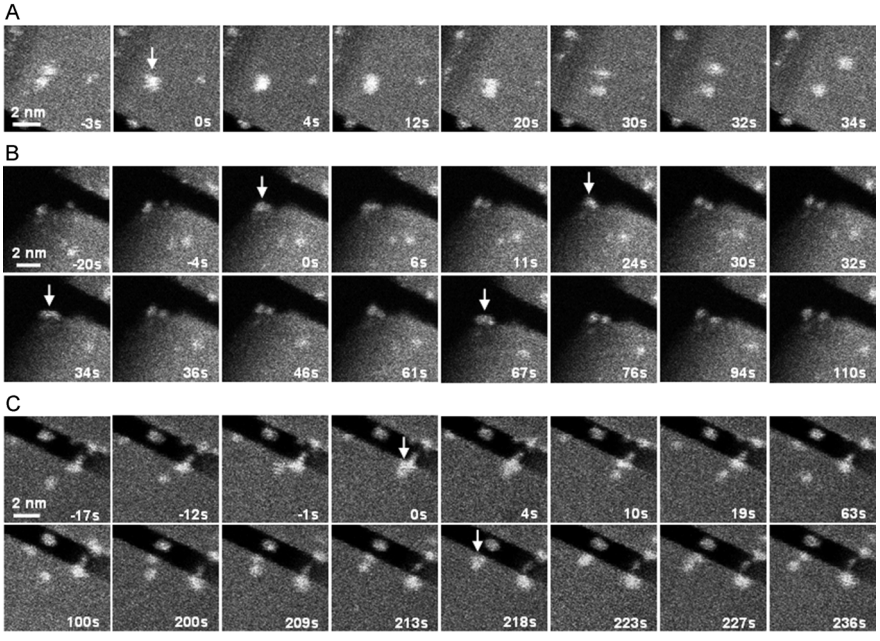

Figure 4. Sequences of HAADF-STEM images showing lack of coalescence of iridium clusters with diameters of approximately 1 nm on MgO. A) Collision of two clusters. B) Multiple collisions of two clusters. C) A cluster colliding with two clusters. The white arrows indicate the collisions, and the time for the first collision is set arbitrarily to be 0. The electron doses received by the sample during the imaging time were approximately (10^5–10^6) e^- Å^{-2}, (10^6–10^7) e^- Å^{-2}, and (10^6–10^7) e^- Å^{-2} for sequences (A), (B), and (C), respectively (see the Supporting Information for details of the dose calculations).

of the sample (Figure 2, Figure 3, Figure 4, and Movies S1–S3 in the Supporting Information). Under the influence of the electron beam, aggregation of the iridium started immediately. After 30 s, the images show a mixture of isolated Ir atoms (encircled in white, Figure 2), clusters of a few Ir atoms each, and aligned Ir atoms evidently en route to cluster formation (indicated with arrows, Figure 2).

Figure 3 shows the frames from a movie of a region of the sample initially containing iridium complexes (with a total beam illumination time of 7 min). The diameters of the iridium species are shown in Figure 3 E and F, illustrating the evolution of the size distribution. Cluster growth was fast during the first 2 min when isolated mononuclear iridium species were abundant, slowing down markedly as clusters formed and these isolated species were depleted. The images in Figure 3 show that after 7 min of electron beam exposure, the majority of the iridium species were nanoclusters about 1 nm in diameter, along with a few mononuclear iridium species and smaller growing clusters. The critical diameter of 1 nm matches that observed for the H_2-treated sample, indicating that it is independent of the treatment and corresponds to an energy minimum.

To investigate the dynamics of the changes and seek an explanation for the stability of the clusters, we analyzed frames of the movie characterizing various regions of the sample (Movie S1–S3 in the Supporting Information). The iridium nanoclusters were highly mobile on the MgO, and collisions between clusters were frequent. Although coalescence of Ir atoms and nanoclusters of subcritical size was rapid, clusters of the critical diameter did not coalesce (Figure 4, Movie S1–S3 in the Supporting Information). In some cases, pairs of clusters of the critical size were observed to undergo multiple fruitless collisions (Figure 4 B); some of these clusters collided with one cluster right after another without coalescence (Figure 4 C).

Calculations at the level of density functional theory (DFT)[32] show

that bare iridium clusters with nuclearities up to 48 Ir atoms (corresponding to diameters less than about 1.1 nm[26]) adopt rigid cubic structures. The coalescence of two of these rigid clusters is prevented because it would require energetically unfavorable rearrangements of the surface atoms. The theoretical results account for our observations showing that iridium clusters of approximately 1 nm in diameter are resistant to aggregation. Indeed, our images confirm the stability of iridium nanoclusters that are cubic, as illustrated by the atomically resolved images of Figures 2 and 3 depicting a few clusters with rectangular surfaces, including a cluster with a square (4×4)-atom face (Figure 2 inset). Such small cubic clusters have high surface-to-volume ratios (e.g., a cubic cluster with 48 atoms has 92% of its atoms on the surface), consistent with its high catalytic activity (Figure 1C).

Besides the mechanism involving migration of nanoclusters on the support surface followed by coalescence that is demonstrated by our observations, there is another commonly discussed mechanism for the growth of supported transition-metal nanoclusters; it is Ostwald ripening, whereby metal atoms are transferred through the vapor phase. This is the more favorable process when the metal–metal interactions are weaker than the metal–support interactions.[33–37] There is no STEM technique to allow direct observations of Ostwald ripening with samples in an atmosphere of H_2 that can exclude electron beam effects, but the evidence weighs strongly against the ripening mechanism in our experiments—because if there had been vapor-phase transport of Ir atoms, some of them very likely would have formed isolated species on the support—but the images characterizing the samples after treatments in H_2 at 353, 673, and even 873 K (Figure 1 and Figures S1 and S2 in the Supporting Information) do not show any isolated Ir atoms on the support.

Thus, we infer that the cluster growth involved surface migration and coalescence. On the basis of kinetics of the growth of ligated iridium nanoclusters in contact with a solvent and characterized by rates of a catalytic reporter reaction, Watzky and Finke[38] proposed the mechanism given in Equations (1–3) for cluster growth:

$$n\,M_1 \rightarrow M_n \qquad \text{nucleation} \qquad (1)$$

$$M_1 + M_n \rightarrow M_{n+1} \qquad \text{cluster buildup} \qquad (2)$$

$$M_m + M_n \rightarrow M_{m+n} \qquad \text{agglomerative cluster growth} \qquad (3)$$

Here, M_1 represents a metal atom (ligands are not shown) and M_m or M_n clusters with nuclearity m or n. The first two steps of this mechanism dominate iridium nanocluster formation, either on a support[39] or in a solvent.[40] In contrast, the growth of platinum nanoclusters depends on all three steps.[41] It was shown[42] that in the case of iridium cluster growth under mild H_2 reduction conditions (295 K), the nucleation step (1) is slow relative to the cluster buildup step (2), and the latter involves changes occurring both on the support surface and in the neighboring solvent, in which the iridium complexes are soluble.[42] The resultant nanoclusters are larger (with an average diameter of approximately 3 nm) than the clusters of approximately 1 nm in diameter described here (and lack the uniform size distribution), raising the question of why our clusters of approximately 1 nm in diameter are uniquely stable.

We interpret the difference as follows: our Ir/MgO samples, in the absence of a solvent and treated under harsher conditions than those of Watzky and Finke, underwent a fast change corresponding to step (1; nucleation), consuming most of the mononuclear iridium species and forming iridium nanoclusters. After as little as 60 s of electron beam exposure, all but a few mononuclear iridium species had been consumed (Figure 3), whereupon the stepwise surface cluster buildup of step (2) became much less significant. The result of further treatment was a population of nanoclusters limited in diameter to approximately 1 nm because these do not coalesce with each other and there was a lack of unstable mononuclear iridium species to combine with them (Scheme 1). Thus, we infer that a treatment that rapidly consumes the unstable catalyst precursor species is essential to the preparation of this sinter-resistant catalyst.

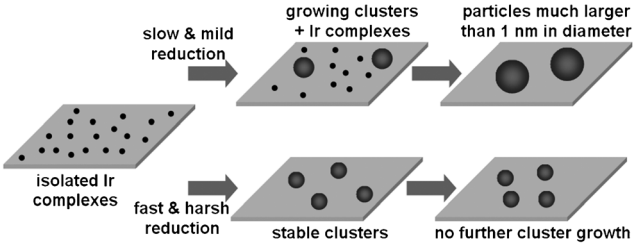

Scheme 1. Cluster formation mechanisms starting from supported iridium complex precursors.

To rule out the possibility that our observations could be interpreted as an indication of a unique influence of the MgO support, we prepared samples from the same precursor ($Ir(C_2H_4)_2(acac)$) and other supports, γ-Al_2O_3 and HY zeolite. The STEM images (Figures S4 and S7 in the Supporting Information) show the distribution of cluster diameters (0.97 ± 0.16 nm and 1.05 ± 0.22 nm for the γ-Al_2O_3- and zeolite-supported samples, respectively) after treatment in H_2 at 673 K for 8 h. The cluster diameters match those of the MgO-supported samples. Furthermore, sequences of images show the lack of coalescence of the iridium clusters of approximately 1 nm in diameter on γ-Al_2O_3 (Figures S5 and S6 in the Supporting Information). Thus, the results show that the stability of the iridium clusters is an intrinsic property of the iridium, independent of the support. This support-independent non-coalescence of the iridium nanoclusters of approximately 1 nm in diameter is consistent with the DFT calculations[32] for the bare iridium clusters.

The high stability of the critically sized clusters is in contrast to the tendency of other catalytically important noble metals, such as platinum, rhodium, and gold, to coalesce readily and form particles much larger than the iridium nanoclusters of approximately 1 nm in diameter[43]—these larger particles are metallic and generally have catalytic properties markedly different from those of nanoclusters,

with the cutoff in properties typically being at a diameter of about 2 nm.[44]

An example of the formation of metal nanoparticles larger than 1 nm in diameter is provided by the work of Herzing et al.,[45] who observed that treatment in air at 393 K for 16 h caused their catalyst, which initially consisted of $HAuCl_4$ on an FeO_x support, to form non-uniform gold particles with diameters ranging from 2 to 15 nm, with an average of 5.4 nm. José-Yacamán et al.[46] showed that, during coalescence, the surface atoms of gold nanoparticles are liquid-like, facilitating coalescence. DFT calculations[47] suggest that this liquid-like property is a consequence of the similar energies of cluster isomers with various arrangements of gold surface atoms.

To show that the observed stability of the iridium clusters of approximately 1 nm in diameter is characteristic of this metal, we prepared MgO-supported samples from $Au(CH_3)_2$(acac) and $Pt(acac)_2$,[23] with essentially the same sample preparation methods that were applied for the supported iridium samples. These gold and platinum samples were treated in H_2 and in the electron beam under conditions identical to those applied in the experiments with the iridium samples, and they were expected to form particles much larger than 1 nm in diameter. Consistent with the expectation, after the H_2 treatment, the STEM images showed that gold and platinum particles had formed in the respective samples, with diameters ranging from 2 to 5 nm, containing between approximately 300 and 4000 metal atoms each[26] (Figures S8 and S10 in the Supporting Information). When the initially prepared supported gold and supported platinum samples were observed in the STEM, the metals aggregated rapidly. After depletion of the mononuclear species, the agglomeration continued as a result of collision and coalescence of the gold and platinum clusters (Figures S9 and S11 the Supporting Information). Thus, these experiments show the sharp contrast in sintering behavior between iridium and the other metals and confirm that it is proper to infer the unique stability of the iridium clusters.

In summary, the results characterizing the supported iridium catalyst are the first experimental demonstration of non-coalescence behavior of supported nanoclusters. The unique stability of iridium nanoclusters of approximately 1 nm in diameter matches theoretical predictions[32] and distinguishes iridium from other noble metals. The iridium nanoclusters are highly active catalysts, with the nanoclusters of 1 nm in diameter being in the size range that favors naphthene ring-opening reactions.[18–22] Our observations may contribute to new approaches to the design of "smart", sinter-resistant catalysts that could include iridium-containing bimetallics.

Experimental Section

Supported iridium, gold, and platinum complexes were prepared by reaction of $Ir(C_2H_4)_2$(acac), $Au(CH_3)_2$(acac), or $Pt(acac)_2$ with calcined MgO, γ-Al_2O_3, or HY zeolite. Each sample contained 1 wt % noble metal. All sample handling was done to exclude air and moisture. STEM images were obtained with a JEOL JEM-2100F electron microscope equipped with a field emission gun (FEG), operating at 200 kV, with a CEOS hexapole probe (STEM) aberration corrector. Details of the experiments are given in the Supporting Information.

Received: March 3, 2012
Published online: April 19, 2012

Keywords: cluster compounds · heterogeneous catalysis · iridium · supported catalysts · surface chemistry

[1] P. J. F. Harris, E. D. Boyes, J. A. Cairns, *J. Catal.* **1983**, *82*, 127–146.
[2] M. A. Newton, *Chem. Soc. Rev.* **2008**, *37*, 2644–2657.
[3] J. Climent, A. Corma, S. Iborra, *Chem. Rev.* **2011**, *111*, 1072–1133.
[4] R. M. J. Fiedorow, S. E. Wanke, *J. Catal.* **1976**, *43*, 34–42.
[5] J. Sá, A. Goguet, S. F. R. Taylor, R. Tiruvalam, C. J. Kiely, M. Nachtegaal, G. J. Hutchings, C. Hardacre, *Angew. Chem.* **2011**, *123*, 9074–9078; *Angew. Chem. Int. Ed.* **2011**, *50*, 8912–8916.
[6] Y. Nishihata, J. Mizuki, T. Akao, H. Tanaka, M. Uenishi, M. Kimura, T. Okamoto, N. Hamadak, *Nature* **2002**, *418*, 164–167.
[7] Y. Nagai, T. Hirabayashi, K. Dohmae, N. Takagi, T. Minami, H. Shinjoh, S. Matsumoto, *J. Catal.* **2006**, *242*, 103–109.
[8] S. J. Tauster, S. C. Fung, R. T. K. Baker, J. A. Horsley, *Science* **1981**, *211*, 1121–1125.
[9] P. M. Arnal, M. Comotti, F. Schüth, *Angew. Chem.* **2006**, *118*, 8404–8407; *Angew. Chem. Int. Ed.* **2006**, *45*, 8224–8227.
[10] S. H. Joo, J. Y. Park, C.-K. Tsung, Y. Yamada, P. Yang, G. A. Somorjai, *Nat. Mater.* **2009**, *8*, 126–131.
[11] P. Botella, A. Corma, M. T. Navarro, M. Quesada, *J. Mater. Chem.* **2009**, *19*, 3168–3175.
[12] S. Liang, J. Li, M. Yu, C. N. McMurray, J. L. Falconer, A. W. Weimer, *ACS Catal.* **2011**, *1*, 1162–1165.
[13] J.-P. Frank, G. P. Martino in *Deactivation and Poisoning of Catalysts* (Eds.: J. Oudar, H. Wise), Marcel Dekker, New York, **1985**, pp. 237–243.
[14] R. H. Crabtree, *Top. Organomet. Chem.* **2011**, *34*, 1–10.
[15] M. Diéguez, O. Pamies, C. Claver, *Top. Organomet. Chem.* **2011**, *34*, 11–29.
[16] J. Choi, A. H. R. MacArthur, M. Brookhart, A. S. Goldman, *Chem. Rev.* **2011**, *111*, 1761–1779.
[17] J. Moran, A. Preetz, R. A. Mesch, M. J. Krische, *Nat. Chem.* **2011**, *3*, 287–290.
[18] F. G. Gault, *Adv. Catal.* **1981**, *30*, 1–95.
[19] W. C. Baird, Jr., J. G. Chen, G. B. McVicker, US Patent 6 623 626, **2003**.
[20] W. C. Baird, Jr., D. P. Klein, M. S. Touvelle, J. G. Chen, G. B. McVicker, US Patent 6 586 650, **2003**.
[21] G. B. McVicker, M. Daage, M. S. Touvelle, C. W. Hudson, D. P. Klein, W. C. Baird, Jr., B. R. Cook, J. G. Chen, S. Hantzer, D. E. W. Vaughan, E. S. Ellis, O. C. Feeley, *J. Catal.* **2002**, *210*, 137–148.
[22] G. B. McVicker, R. T. K. Baker, R. L. Garten, E. L. Kugler, *J. Catal.* **1980**, *65*, 207–220.
[23] Both precursors are similar in reactivity to $Ir(C_2H_4)_2$(acac). The acac ligands are readily removed by reaction with the support surface hydroxy groups, leading to the formation of chemisorbed mononuclear iridium species. Details of the sample synthesis chemistry can be found in J. Guzman, B. C. Gates, *Dalton Trans.* **2003**, 3303–3318.
[24] A. Uzun, V. Ortalan, N. D. Browning, B. C. Gates, *J. Catal.* **2010**, *269*, 318–328.
[25] J. Lu, P. Serna, C. Aydin, N. D. Browning, B. C. Gates, *J. Am. Chem. Soc.* **2011**, *133*, 16186–16196.
[26] Y. Lin, R. G. Finke, *J. Am. Chem. Soc.* **1994**, *116*, 8335–8353.

[27] N. L. Okamoto, B. W. Reed, S. Mehraeen, A. Kulkarni, D. G. Morgan, B. C. Gates, N. D. Browning, *J. Phys. Chem. Lett.* **2008**, *112*, 1759 – 1763.
[28] A. Jentys, *Phys. Chem. Chem. Phys.* **1999**, *1*, 4059 – 4063.
[29] A. Uzun, B. C. Gates, *J. Am. Chem. Soc.* **2009**, *131*, 15887 – 15894.
[30] K. Song, D. J. Sauter, J. Wu, V. P. Dravid, P. C. Stair, *ACS Catal.* **2012**, *2*, 384 – 390.
[31] C. Aydin, J. Lu, A. J. Liang, C.-Y. Chen, N. D. Browning, B. C. Gates, *Nano Lett.* **2011**, *11*, 5537 – 5541.
[32] T. Pawluk, Y. Hirata, L. Wang, *J. Phys. Chem. B* **2005**, *109*, 20817 – 20823.
[33] M. von Smoluchowski, *Z. Phys. Chem.* **1918**, *92*, 129 – 168.
[34] P. J. F. Harris, *Int. Mater. Rev.* **1995**, *40*, 97 – 115.
[35] P. Jensen, *Rev. Mod. Phys.* **1999**, *71*, 1695 – 1735.
[36] T. T. Tsong, *Prog. Surf. Sci.* **2001**, *67*, 235 – 248.
[37] D.-Q. Yang, E. Sacher, *Appl. Surf. Sci.* **2003**, *207*, 1 – 5.
[38] M. A. Wakzty, R. G. Finke, *J. Am. Chem. Soc.* **1997**, *119*, 10382 – 10400.
[39] J. E. Mondloch, Q. Wang, A. I. Frenkel, R. G. Finke, *J. Am. Chem. Soc.* **2010**, *132*, 9701 – 9714.
[40] M. A. Wakzty, E. E. Finney, R. G. Finke, *J. Am. Chem. Soc.* **2008**, *130*, 11959 – 11969.
[41] C. Besson, E. E. Finney, R. G. Finke, *J. Am. Chem. Soc.* **2005**, *127*, 8179 – 8184.
[42] J. E. Mondloch, R. G. Finke, *J. Am. Chem. Soc.* **2011**, *133*, 7744 – 7756.
[43] S. E. Wanke, P. C. Flynn, *Catal. Rev.* **1975**, *12*, 93 – 135.
[44] J. K. Nørskov, F. Aild-Pedersen, F. Studt, T. Bligaard, *Proc. Natl. Acad. Sci. USA* **2011**, *108*, 937 – 943.
[45] A. A. Herzing, C. J. Kiely, A. F. Carley, P. Landon, G. J. Hutchings, *Science* **2008**, *321*, 1331 – 1335.
[46] M. José-Yacamán, C. Gutierrez-Wing, M. Miki, D.-Q. Yang, K. N. Piyakis, J. Sacher, *J. Phys. Chem. B* **2005**, *109*, 9703 – 9711.
[47] L. Xiao, L. Wang, *J. Phys. Chem. A* **2004**, *108*, 8605 – 8614.

